





# Inelastic neutron scattering studies on the eight-spin zigzag-chain compound $\text{KCu}_4\text{P}_3\text{O}_{12}$ : Confirmation of the validity of a data-driven technique based on machine learning

Masashi Hase <sup>1,\*</sup>, Ryo Tamura <sup>2,3</sup>, Koji Hukushima <sup>4,5</sup>, Shinichiro Asai,<sup>6</sup>  
Takatsugu Masuda,<sup>6</sup> Shinichi Itoh,<sup>7</sup> and Andreas Dönni <sup>1</sup>

<sup>1</sup>Research Center for Materials Nanoarchitectonics (MANA), National Institute for Materials Science (NIMS),  
1-1 Namiki, Tsukuba, Ibaraki 305-0044, Japan

<sup>2</sup>Center for Basic Research on Materials (CBRM), National Institute for Materials Science (NIMS),  
1-1 Namiki, Tsukuba, Ibaraki 305-0044, Japan

<sup>3</sup>Graduate School of Frontier Sciences, The University of Tokyo, 5-1-5 Kashiwanoha, Kashiwa, Chiba 277-8568, Japan

<sup>4</sup>Komaba Institute for Science, The University of Tokyo, 3-8-1 Komaba, Meguro, Tokyo 153-8902, Japan

<sup>5</sup>Department of Basic Science, Graduate School of Arts and Sciences, The University of Tokyo, 3-8-1 Komaba, Meguro, Tokyo 153-8902, Japan

<sup>6</sup>The Institute for Solid State Physics (ISSP), The University of Tokyo, 5-1-5 Kashiwanoha, Kashiwa, Chiba 277-8581, Japan

<sup>7</sup>Institute of Materials Structure Science (IMSS), High Energy Accelerator Research Organization (KEK),  
1-1 Oho, Tsukuba, Ibaraki 305-0801, Japan



(Received 16 October 2023; accepted 8 March 2024; published 25 March 2024)

We performed inelastic neutron scattering (INS) experiments on  $\text{KCu}_4\text{P}_3\text{O}_{12}$  powder and compared the experimental results with those calculated for the spin model (an eight-spin zigzag chain with  $S = \frac{1}{2}$ ) using the data-driven technique based on machine learning. We observed magnetic excitations at approximately 3.0, 4.1, 5.9, and 8.8 meV at 5.5 K and at approximately 3.8 and 5.9 meV at 49 K. The excitations corresponding to 3.0, 4.1, and 8.8 meV were magnetic excitations from the ground state to the first, second, and fourth excited states (2.87, 4.23, and 8.53 meV from the calculations), respectively. The excitations corresponding to 3.8 and 5.9 meV were magnetic excitations from the first excited state to the third and fourth excited states (3.78 and 5.67 meV from the calculations), respectively. An excitation was likely to exist between the first and second excited states at approximately 1.35 meV in the experimental results. The excitation energies obtained from the INS experiments were almost consistent with those calculated from the exchange interaction values via the data-driven technique (data-driven values). The experimental  $I(Q)$  curves could not be reproduced. We found that  $I(Q)$  curves could be changed largely by small changes of exchange-interaction values. Therefore, we expect that exchange-interaction values, which can explain not only the magnetic susceptibility, magnetization curves, and excitation energies but also INS intensity, are in the vicinity of the data-driven values.

DOI: [10.1103/PhysRevB.109.094434](https://doi.org/10.1103/PhysRevB.109.094434)

## I. INTRODUCTION

The precise knowledge of exchange interactions is a prerequisite for understanding the magnetic properties of quantum spin systems. Typically, exchange interactions are evaluated by analyzing the magnetic susceptibility and magnetization curves. However, it is often difficult to uniquely evaluate multiple exchange interactions. For example, several sets of exchange interaction values have been reported for the diamond chain compound  $\text{Cu}_3(\text{CO}_3)_2(\text{OH})_2$  [1–8] and the dimer-monomer compound  $\text{Ni}_2\text{V}_2\text{O}_7$  [9–12].

Tamura and Hukushima have developed a data-driven technique based on machine learning to evaluate multiple exchange interactions and their uncertainty from multiple physical quantities [13,14]. This data-driven technique was based on Bayesian statistics, and the exchange interactions were determined such that the posterior distribution was maximized. The posterior distribution constitutes the difference between the experimental and calculated results obtained

using an effective model and appropriate prior distribution of exchange interactions. The prior distribution corresponds to prior knowledge of the target material.

Recently, this data-driven technique based on machine learning was applied to  $\text{KCu}_4\text{P}_3\text{O}_{12}$  [15]. In this compound, the  $\text{Cu}^{2+}$  ions possess  $S = \frac{1}{2}$  spins. Figure 1 shows the spin model (an eight-spin zigzag chain) based on the crystal structure [16]. The spin Hamiltonian is defined as  $-\sum_{i=1}^7 J_{i,i+1} \mathbf{S}_i \mathbf{S}_{i+1}$ , where  $J_1 = J_{1,2} = J_{7,8}$ ,  $J_2 = J_{2,3} = J_{6,7}$ ,  $J_3 = J_{3,4} = J_{5,6}$ , and  $J_4 = J_{4,5}$ . Using the magnetic susceptibility and magnetization curves at various temperatures, we evaluated the exchange interactions as follows:  $J_1 = -8.54 \pm 0.51$  meV [antiferromagnetic (AFM)],  $J_2 = -2.67 \pm 1.13$  meV (AFM),  $J_3 = -3.90 \pm 0.15$  meV (AFM), and  $J_4 = 6.24 \pm 0.95$  meV [ferromagnetic (FM)] [15]. We used the values of the exchange interactions to calculate the excitation energies of the magnetic excitations. The excitation energies of the low-lying eigenstates are listed in Table I. Figure 2 shows the histogram of the excitation energies.

To demonstrate that the data-driven technique based on machine learning is an important tool for scientific research,

\*HASE.Masashi@nims.go.jp

TABLE I. Low-lying eigenstates in the spin model of  $\text{KCu}_4\text{P}_3\text{O}_{12}$ .  $S$  denotes the total spin of the eigenstates. Excitation energies were evaluated from  $J_1 = -8.54 \pm 0.51$ ,  $J_2 = -2.67 \pm 1.13$ ,  $J_3 = -3.90 \pm 0.15$ , and  $J_4 = 6.24 \pm 0.95$  meV determined by the data-driven technique based on machine learning (Cal1) and  $J_1 = -8.71$ ,  $J_2 = -3.89$ ,  $J_3 = -4.00$ , and  $J_4 = 4.27$  meV determined by a steepest descent method (Cal2) described in the Sec. III. We evaluated uncertainties of the Cal1 results from the uncertainties of the exchange-interaction values as is shown in Fig. 2. We also show the excitation energies estimated from the INS results. The magnetic excitations indicated by the symbol ‘‘O’’ are experimentally observed. The excitation between GS and 3ES is forbidden (‘‘F’’). We estimated the excitation energy between GS and 3ES from that between GS and 1ES and that between 1ES and 3ES.

	$S$	Excitation energy (meV)			Observation	
		Cal1	Cal2	Exp	From GS	From 1ES
GS	0	0	0	0		
1ES	1	$2.87 \pm 0.11$	3.02	$3.0 \pm 0.2$	O	
2ES	1	$4.23 \pm 0.13$	4.17	$4.1 \pm 0.5$	O	O
3ES	2	$6.65 \pm 0.21$	6.75	$6.8 \pm 0.3$	F	O
4ES	1	$8.53 \pm 0.30$	8.80	$8.8 \pm 0.5$	O	O

it is necessary to confirm that other physical quantities (particularly the microscopic quantities) of  $\text{KCu}_4\text{P}_3\text{O}_{12}$  can be reproduced using the spin model. We can determine the excitation energies of the magnetic excitations using inelastic neutron scattering (INS) measurements and compare the experimental excitation energies with the calculated excitation energies. Accordingly, we performed INS measurements on  $\text{KCu}_4\text{P}_3\text{O}_{12}$  powder.

## II. EXPERIMENTAL METHODS

We synthesized a crystalline powder of  $\text{KCu}_4\text{P}_3\text{O}_{12}$  via solid-state reaction. The starting materials were  $\text{K}_2\text{CO}_3$ , CuO, and  $(\text{NH}_4)_2\text{HPO}_4$  powders with purities of 99.9%, 99.99%, and 99%, respectively. A stoichiometric mixture of the powders was calcined at 523 K for 48 h in air. The calcined powders were sintered at 973 K for 168 h in air. In Ref. [16], fabrication of single crystals with diameters up to 0.3 mm using hydrothermal synthesis was reported. Many samples (typically 10 g) are necessary for neutron scattering experiments. Therefore, we used the solid-state reaction. X-ray powder diffraction patterns were recorded at room temperature using an x-ray diffractometer (RINT-TTR III, Rigaku). We performed Rietveld refinements of the crystal structure using the FULLPROF Suite software package containing

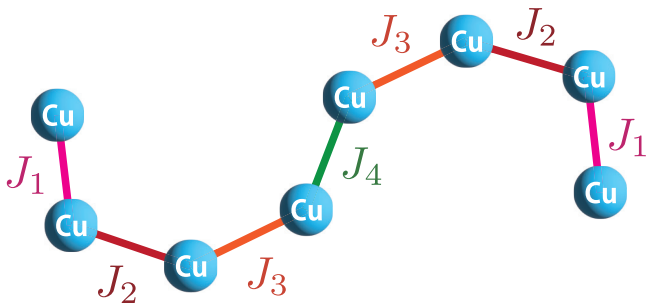


FIG. 1. Schematic of the spin model (an eight-spin zigzag chain) in  $\text{KCu}_4\text{P}_3\text{O}_{12}$  [15,16] drawn using VESTA [17]. Using the data-driven technique based on machine learning, the exchange interactions were evaluated as  $J_1 = -8.54 \pm 0.51$  meV (AFM),  $J_2 = -2.67 \pm 1.13$  meV (AFM),  $J_3 = -3.90 \pm 0.15$  meV (AFM), and  $J_4 = 6.24 \pm 0.95$  meV (FM).

internal tables for the scattering lengths [18]. We used a physical property measurement system (Quantum Design) for specific heat measurements. We performed INS measurements using the High Resolution Chopper (HRC) spectrometer at BL 12 at the Japan Proton Accelerator Research Complex (J-PARC) [19–21].

## III. RESULTS AND DISCUSSIONS

The blue circles in Fig. 3 represent the x-ray diffraction pattern of  $\text{KCu}_4\text{P}_3\text{O}_{12}$  at room temperature. The line on the experimental pattern shows the results of the Rietveld refinements using the crystal structure reported in Ref. [16]. This line is consistent with the experimental results.

The red circles in Fig. 4 show the temperature  $T$  dependence of the specific heat  $[C(T)]$  of  $\text{KCu}_4\text{P}_3\text{O}_{12}$ . No phase transition appears between 1.9 and 300 K. The blue circles in

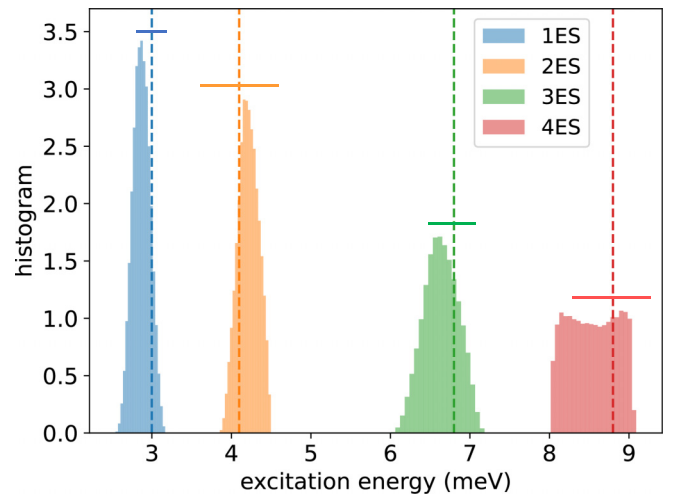


FIG. 2. The histogram of the excitation energy evaluated from  $J_1 = -8.54 \pm 0.51$ ,  $J_2 = -2.67 \pm 1.13$ ,  $J_3 = -3.90 \pm 0.15$ , and  $J_4 = 6.24 \pm 0.95$  meV determined by the data-driven technique based on machine learning. We divided the uncertainty range into 20 equal parts for each exchange-interaction value and calculated eigenenergies for 194 481 ( $= 21^4$ ) sets of the exchange interactions. Vertical and horizontal lines show the excitation energies and their uncertainties, respectively, estimated from the INS results.

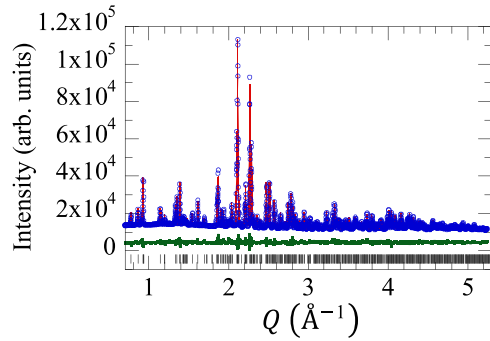


FIG. 3. X-ray diffraction pattern (circles) of  $\text{KCu}_4\text{P}_3\text{O}_{12}$  at room temperature. The line on the measured pattern portrays the Rietveld-refined pattern obtained using the crystal structure with  $P\bar{1}$  (No. 2) [16]. The line at the bottom portrays the difference between the measured and Rietveld-refined patterns. The hash marks represent the positions of reflections. The lattice constants are  $a = 7.4273(2)$  Å,  $b = 7.8327(2)$  Å,  $c = 9.4573(2)$  Å,  $\alpha = 108.285(1)^\circ$ ,  $\beta = 112.671(1)^\circ$ , and  $\gamma = 92.743(1)^\circ$ . The reliability indices of the refinements are  $R_p = 1.82\%$ ,  $R_{wp} = 2.43\%$ , and  $R_{exp} = 0.82\%$ .

Fig. 4(b) represent  $C(T)$  of the spin model with the exchange-interaction values described in Fig. 1. The experimental and calculated specific heats are consistent with each other below 10 K where the lattice specific heat is probably small. The calculated specific heat has a broad maximum at around 30 K. The broad maximum is not seen in the experimental  $C(T)$  probably due to overlap of the lattice specific heat. Accordingly, we cannot prove that the exchange-interaction values are correct for  $\text{KCu}_4\text{P}_3\text{O}_{12}$  by the  $C(T)$  result.

Figure 5 shows the INS intensity  $I(Q, \omega)$  maps of  $\text{KCu}_4\text{P}_3\text{O}_{12}$  powder below 7.0 meV at various temperatures.

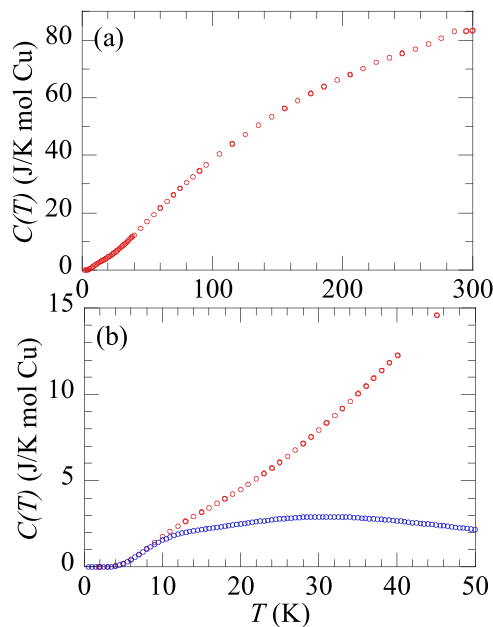


FIG. 4. Temperature  $T$  dependence of the specific heat  $C(T)$  of  $\text{KCu}_4\text{P}_3\text{O}_{12}$  (red circles). The blue circles in panel (b) indicate  $C(T)$  calculated for the spin model with  $J_1 = -8.54$ ,  $J_2 = -2.67$ ,  $J_3 = -3.90$ , and  $J_4 = 6.24$  meV.

Here,  $Q$  and  $\omega$  denote the magnitudes of the scattering vector and the energy transfer, respectively. The energy of the incident neutrons ( $E_i$ ) is 15.3 meV. At 5.5 K, strong excitations at approximately 3.0 meV and weak excitations up to 6.0 meV are observed. The 3.0-meV excitation exists over a wide  $Q$  range, indicating a cluster excitation. The intensities of the excitations decrease with increasing  $T$ ; therefore, they are magnetic in nature. Figure 6 shows the  $I(Q, \omega)$  maps up to 15.0 meV at 5.5 K. The value of  $E_i$  is 25.4 meV. Another magnetic excitation exists at approximately 8.8 meV.

Figure 7 shows the  $\omega$  dependence of the INS intensity  $I(\omega)$  at  $E_i = 15.3$  meV. Magnetic excitations are observed at approximately 3.0, 4.1, 5.9, and 8.8 meV at 5.5 K as shown in Figs. 7(a) and 7(b) and at approximately 3.8 and 5.9 meV at 49 K as shown in Fig. 7(e). The horizontal bars indicate the energy resolution. The value at  $\omega = 0$  meV ( $\Delta\omega_0$ ) is 0.855 meV. We assumed that the energy resolution at a finite  $\omega$  was  $\Delta\omega_0(1 - \omega/E_i)^{3/2}$ . The width of the 3.0-meV excitation is slightly greater than the energy resolution. The widths of the other excitations seem greater than the energy resolutions.

Considering the excitation energies from the ground and first excited states (represented by the pink and blue triangles, respectively) calculated for the eight-spin zigzag chain with  $J_1 = -8.54$ ,  $J_2 = -2.67$ ,  $J_3 = -3.90$ , and  $J_4 = 6.24$  meV, the 3.0, 4.1, and 8.8 meV excitations were magnetic excitations from the ground state (GS) to the first, second, and fourth excited states (1ES, 2ES, and 4ES), respectively; we refer to them as the 0-1, 0-2, and 0-4 excitations, respectively. As shown in Table I, the excitation between the GS and the third excited state (3ES) is forbidden. As the temperature increases, the intensity of the 3.0-meV excitation decreases rapidly and the excitation is not observed at 49 K. However, the 5.9-meV excitation is observed at 49 K, as shown in Fig. 7(e). Because the  $T$  dependence of the excitation intensity is determined by the thermal population factor of the initial state [22], excitations from the same initial state exhibit the same  $T$  dependence of the intensity. Therefore, the initial state of the 5.9-meV excitation is not the GS. It is likely that the 5.9-meV excitation is the excitation from 1ES to 4ES (1-4 excitation). Similarly, the initial state of the 3.8-meV excitation at 49 K shown in Fig. 7(e) is not the GS. We consider that the 3.8-meV excitation is the excitation from 1ES to 3ES (1-3 excitation), and the excitations at around 4.0 meV at 5.5 K comprise both the 0-2 and the 1-3 excitations. Four excitations (0-1, 0-2, 1-3, and 1-4 excitations) exist between 2.0 and 6.0 meV. We could not separate them and evaluate the  $T$  dependence of the intensity of each excitation. The intensity between 1.0 and 2.0 meV increases with  $T$ . Therefore, excitations exist in this range and probably include the 1-2 excitation, although we cannot separate the 1-2 excitation. As shown in Table I and Fig. 2, we observed all the low-lying excitations from the GS and 1ES. The excitation energies evaluated by the data-driven technique based on machine learning were almost consistent with those obtained using the INS experiments on  $\text{KCu}_4\text{P}_3\text{O}_{12}$ .

The circles in Fig. 8 represent the  $Q$  dependence of the INS intensity  $I(Q)$  for the 0-1, 0-2, 0-4, 1-3, and 1-4 excitations at  $E_i = 15.3$  meV. We observed an apparent  $Q$  dependence of the experimental  $I(Q)$  except for the  $I(Q)$  for the 0-4 excitation depicted in Fig. 8(c). The pink lines in Fig. 8 denote  $I(Q)$

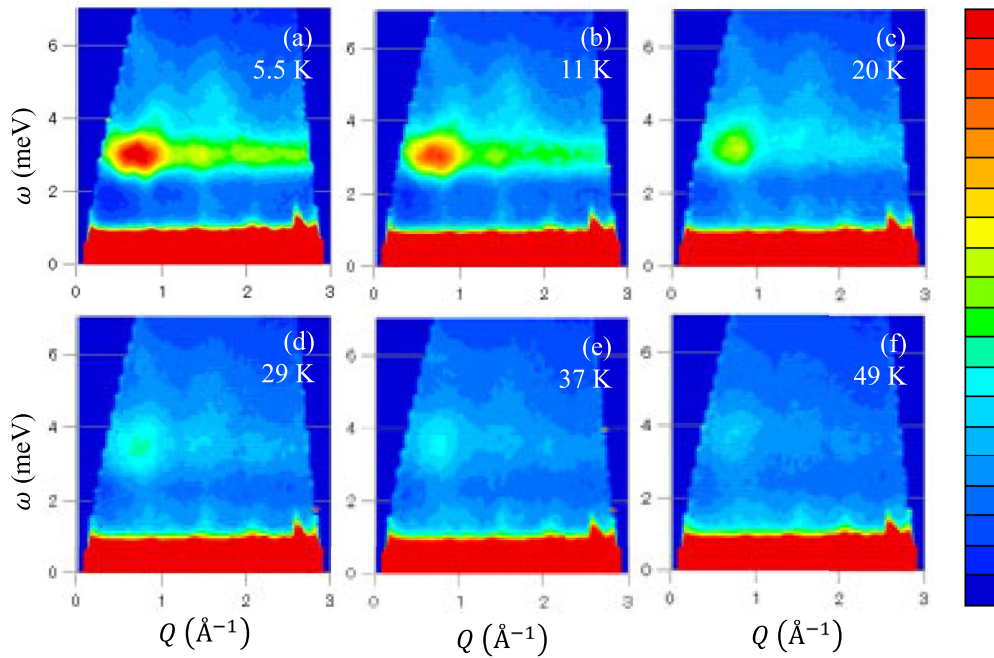


FIG. 5. The INS intensity  $I(Q, \omega)$  maps of  $\text{KCu}_4\text{P}_3\text{O}_{12}$  powder below 7.0 meV at various temperatures. The energy of incident neutrons  $E_i$  is 15.3 meV. The vertical key on the right shows the INS intensity in arbitrary units.

calculated using  $J_1 = -8.54$ ,  $J_2 = -2.67$ ,  $J_3 = -3.90$ , and  $J_4 = 6.24$  meV. The formulas for  $I(Q)$  are described in the Appendix [23–29]. The two peak positions are slightly lower in the experimental  $I(Q)$  curves than in the calculated ones (pink) for the 0-1 and 1-3 excitations. For the 0-4 excitation,

the  $Q$  dependence of the experimental  $I(Q)$  is weaker than that of the calculated  $I(Q)$ . The experimental and calculated  $I(Q)$  curves (pink) for the 0-2 and 1-4 excitations do not agree with each other.

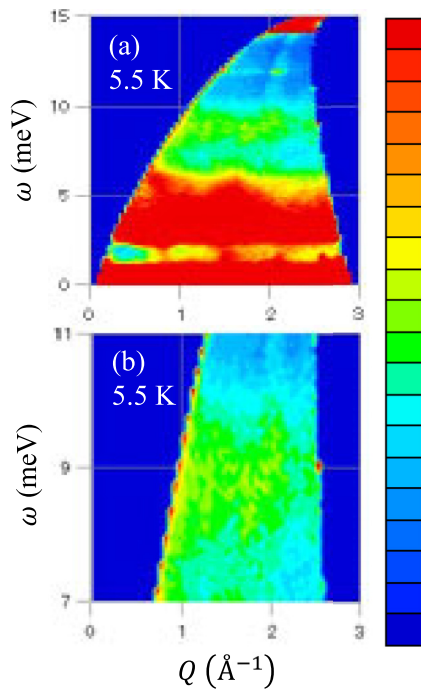


FIG. 6. (a) The INS intensity  $I(Q, \omega)$  map of  $\text{KCu}_4\text{P}_3\text{O}_{12}$  powder below 15.0 meV at 5.5 K. The energy of incident neutrons  $E_i$  is 25.4 meV. The vertical key on the right shows the INS intensity in arbitrary units. (b) Map between 7 and 11 meV.

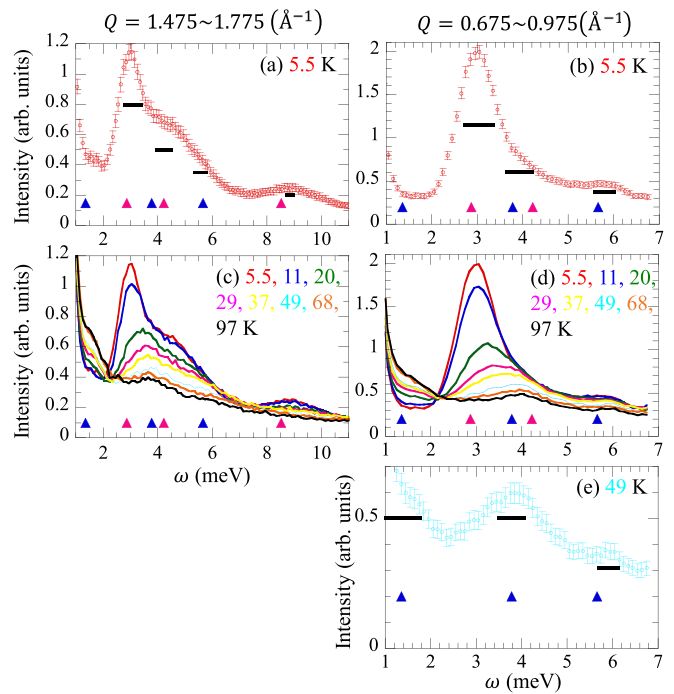


FIG. 7.  $\omega$  dependence of the INS intensity  $I(\omega)$  of  $\text{KCu}_4\text{P}_3\text{O}_{12}$  powder. The energy of the incident neutrons  $E_i$  is 15.3 meV. The pink and blue triangles indicate the excitation energies from the GS and 1ES, respectively. The horizontal bars represent the energy resolution.



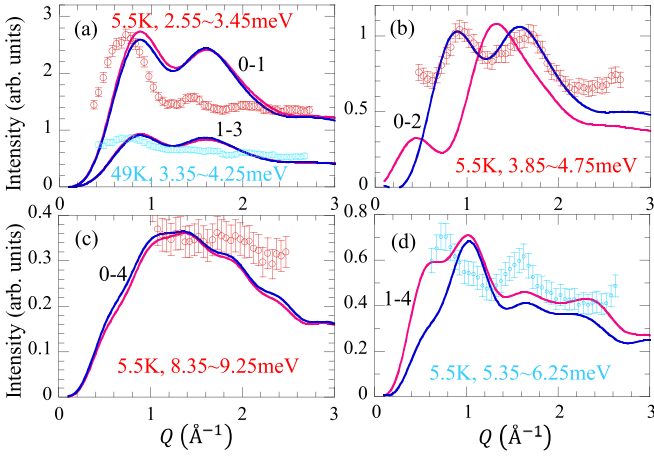


FIG. 8.  $Q$  dependence of the INS intensity  $I(Q)$  of  $\text{KCu}_4\text{P}_3\text{O}_{12}$  powder (circles). The energy of incident neutrons  $E_i$  is 15.3 meV. The lines indicate  $I(Q)$  calculated for (a) the 0-1 and 1-3 excitations, (b) the 0-2 excitation, (c) the 0-4 excitation, and (d) the 1-4 excitation. The pink lines were obtained from  $J_1 = -8.54$ ,  $J_2 = -2.67$ ,  $J_3 = -3.90$ , and  $J_4 = 6.24$  meV evaluated using the data-driven technique based on machine learning [15]. The blue lines were obtained from  $J_1 = -8.71$ ,  $J_2 = -3.89$ ,  $J_3 = -4.00$ , and  $J_4 = 4.27$  meV evaluated using a steepest descent method.

Unlike the case of AFM dimers, we could not utilize the peak positions of  $I(Q)$  to directly determine the Cu-Cu pairs that exhibited strong exchange interactions in  $\text{KCu}_4\text{P}_3\text{O}_{12}$ . This is because  $I(Q)$  consists of multiple terms as described in the Appendix. In an AFM dimer with a spin-spin distance  $R$ ,  $I(Q)$  is expressed as  $f(Q)^2 A [1 - \frac{\sin(QR)}{QR}]$ . We can use the value of  $R$  to determine the Cu-Cu pair that forms an AFM dimer. For example, when the positions of the first peak in the  $I(Q)$  for the 0-1 and 0-2 excitations ( $Q = 0.7$  and  $0.9 \text{ \AA}^{-1}$ , respectively) were matched to those in the  $I(Q)$  of an AFM dimer, we obtained  $R = 6.1$  and  $4.8 \text{ \AA}$ , respectively. In contrast, the spin-spin distances in the four exchange interactions in  $\text{KCu}_4\text{P}_3\text{O}_{12}$  are located between  $2.94$  and  $3.19 \text{ \AA}$ .

The difference in the  $\omega$  dependence of the INS intensity between Figs. 7(a) and 7(b) is mainly caused by the structural factor of the magnetic excitations. As shown in Fig. 8(a), the experimental intensity of the 3.0 meV (0-1) excitation is larger at around  $Q = 0.7 \text{ \AA}^{-1}$  corresponding to Fig. 7(b) than at around  $Q = 1.6 \text{ \AA}^{-1}$  corresponding to Fig. 7(a). Thus, the 4.1-meV (0-2) excitation is less apparent in Fig. 7(b). As shown in Fig. 8(b), the experimental intensity of the 4.1-meV (0-2) excitation is larger at around  $Q = 1.6 \text{ \AA}^{-1}$  than at around  $Q = 0.7 \text{ \AA}^{-1}$ . Thus, the 5.9-meV (1-4) excitation is less apparent in Fig. 7(a).

The inconsistency between the experimental and calculated  $I(Q)$  curves (pink) indicates that the present exchange-interaction values determined by the data-driven technique based on machine learning (data-driven values) are not appropriate. However, to obtain exchange-interaction values that can reproduce quantitatively the INS intensity, we need the INS intensity of magnetic excitation alone. As is seen in Figs. 8(a) and 8(c), the 0-1 and 0-4 excitations show weak  $Q$  dependencies above  $Q = 1 \text{ \AA}^{-1}$ , suggesting that the

contributions of the phonon excitation and background cannot be ignored. However, we could not subtract the contributions because of the lack of information. Accordingly, it is impossible at present to evaluate the exchange interactions from the INS intensity.

Next, we considered evaluations of the exchange interactions from the excitation energies. There may be different sets of exchange-interaction values that can reproduce the magnetic susceptibility, magnetization curves, and excitation energies. However, we cannot determine which set is correct because the experimental results can be also explained by the data-driven values. Therefore, we searched exchange-interaction values, which could reproduce more correctly the excitation energies, using the data-driven values as the starting point. Here, we utilized a steepest descent method to find a local minimum. The results are  $J_1 = -8.71$ ,  $J_2 = -3.89$ ,  $J_3 = -4.00$ , and  $J_4 = 4.27$  meV of which excitation energies are 3.02, 4.17, 6.75, and 8.80 meV from GS to 1ES, 2ES, 3ES, and 4ES, respectively, as described in Table I. The values are close to the experimental values (3.0, 4.1, 6.8, and 8.8 meV, respectively). The new  $J_1$ ,  $J_2$ , and  $J_3$  values are almost within the uncertainties of the data-driven values, whereas the new  $J_4$  value is slightly smaller than the data-driven value. As shown in Fig. 9, the curves calculated using the new values are close to those calculated using the data-driven values. We evaluated differences between the experimental and calculated results. The agreements at the magnetic susceptibility and the magnetization curve at 50 K are slightly better in the results using the new values and those at the magnetization curves between 1.3 and 30 K are slightly better in the results using the data-driven values. On the other hand, as shown in Figs. 8(b) and 8(d), the  $I(Q)$  curves calculated using the new values (blue) are clearly different from those calculated using the data-driven values (pink) in spite of the small differences between the data-driven values and new values. This result suggests that  $I(Q)$  curves can be changed largely by small changes of exchange-interaction values.

As shown in Fig. 8(b), the peak positions and the ratio of intensities between the two peaks of the blue curve calculated using the new values are close to those of the experimental  $I(Q)$  curve, although there are apparent differences between the calculated and experimental  $I(Q)$  curves at  $Q < 0.6$  and  $Q > 2.0 \text{ \AA}^{-1}$  probably due to the contributions of the phonon excitation and background. Therefore, we expect that exchange-interaction values, which can explain not only the magnetic susceptibility, magnetization curves, and excitation energies but also the INS intensity of magnetic excitation alone, are in the vicinity of the data-driven values. In future, we will perform further neutron scattering experiments and obtain the INS intensity of magnetic excitation alone after subtracting the contributions of phonon excitations and the background. Our current simulation code based on the Bayesian statistics does not support INS data. We will develop an algorithm including an investigation of prior distribution for interactions to obtain exchange-interaction values that can reproduce the magnetic susceptibility, magnetization curves, and INS intensities. If we cannot obtain the exchange-interaction values that can reproduce all the experimental results, we will have to consider a model containing other exchange interactions.

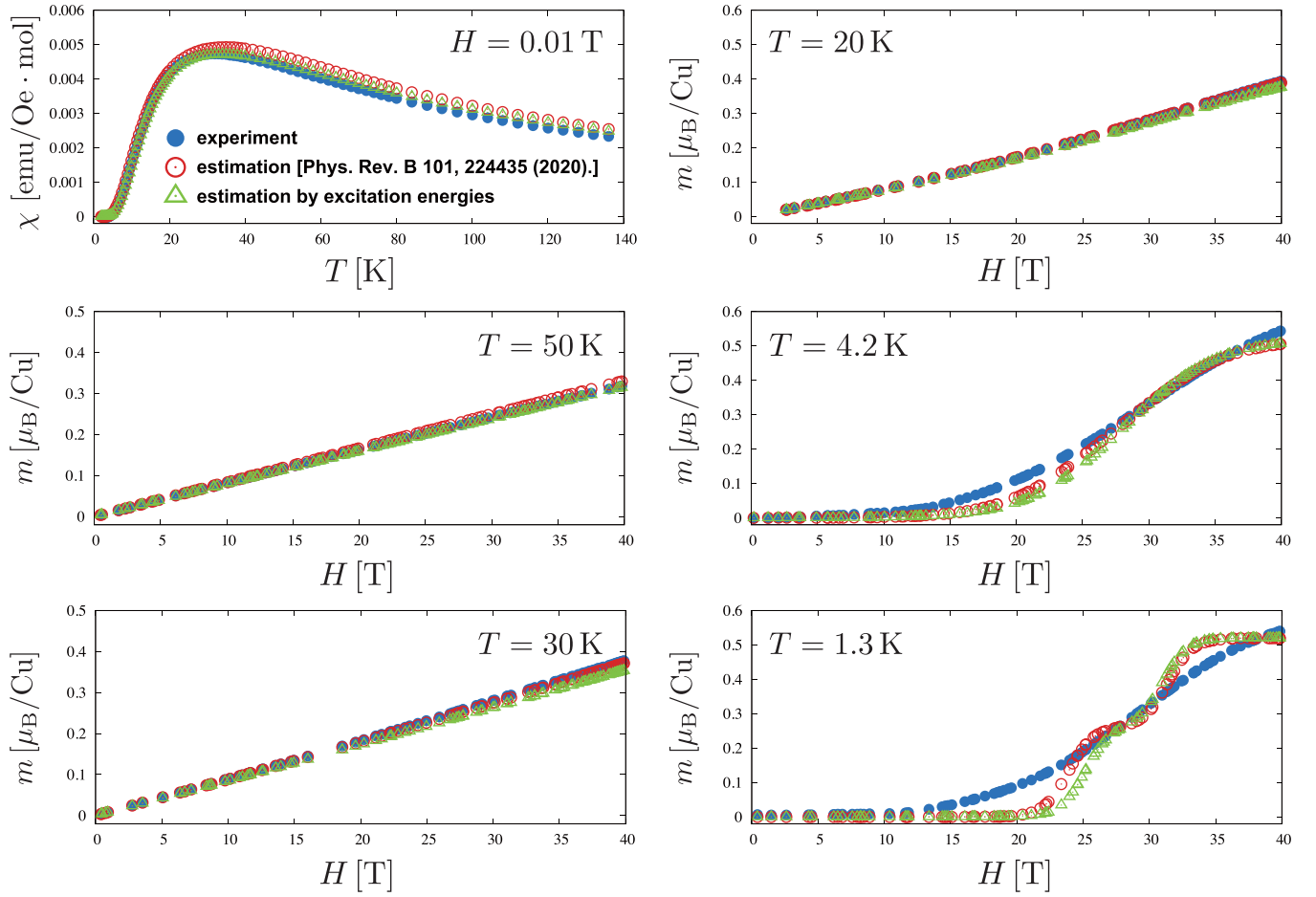


FIG. 9. Comparison plots of the magnetic susceptibility at 0.01 T and the magnetization curves at various temperatures between the experimental (blue circles) and calculated results. The red circles were obtained from  $J_1 = -8.54$ ,  $J_2 = -2.67$ ,  $J_3 = -3.90$ , and  $J_4 = 6.24$  meV evaluated using the data-driven technique based on machine learning [15]. The green triangles were obtained from  $J_1 = -8.71$ ,  $J_2 = -3.89$ ,  $J_3 = -4.00$ , and  $J_4 = 4.27$  meV evaluated using a steepest descent method.

#### IV. CONCLUSION

We performed INS experiments on  $\text{KCu}_4\text{P}_3\text{O}_{12}$  powder and compared the experimental results with those calculated for the spin model (an eight-spin zigzag chain with  $S = \frac{1}{2}$ ) using the data-driven technique based on machine learning. We observed magnetic excitations at approximately 3.0, 4.1, 5.9, and 8.8 meV at 5.5 K and at approximately 3.8 and 5.9 meV at 49 K. The 3.0-, 4.1-, and 8.8-meV excitations were magnetic excitations from the ground state to the first, second, and fourth excited states (2.87, 4.23, and 8.53 meV from the calculations), respectively. The 3.8- and 5.9-meV excitations were magnetic excitations from the first excited state to the third and fourth excited states (3.78 and 5.67 meV from the calculations), respectively. We considered that, in the experimental results, an excitation between the first and second excited states existed at approximately 1.35 meV. The excitation energies obtained from INS experiments almost agree with those calculated from the exchange interaction values evaluated using the data-driven technique. We observed all the low-lying excitations from the ground and first excited states. The experimental  $I(Q)$  curves cannot be reproduced, suggesting that the data-driven values are not appropriate.

Therefore, we searched exchange-interaction values, which could reproduce more correctly the excitation energies, using the data-driven values as the starting point. The newly obtained  $J_1$ ,  $J_2$ , and  $J_3$  values are almost within the uncertainties of the data-driven values, whereas the newly obtained  $J_4$  value is slightly smaller than the data-driven value. We compared the  $I(Q)$  curves calculated using the data-driven values with those calculated using the new values. We found that  $I(Q)$  curves could be changed largely by small changes of exchange-interaction values. Therefore, we expect that exchange-interaction values, which can explain not only the magnetic susceptibility, magnetization curves, and excitation energies but also the INS intensity of magnetic excitation alone, are in the vicinity of the data-driven values.

#### ACKNOWLEDGMENTS

This study was supported by Japanese Society for the Promotion of Science (JSPS) KAKENHI Grant No. 18K03551 and the World Premier International Research Center Initiative (WPI), Ministry of Education, Culture, Sports, Science and Technology (MEXT), Japan. The neutron scattering

experiments on  $\text{KCu}_4\text{P}_3\text{O}_{12}$  were approved by the Neutron Science Proposal Review Committee of J-PARC/MLF (Proposal No. 2020B0026) and supported by the Inter-University Research Program on Neutron Scattering of IMSS, KEK. We thank Seiko Matsumoto at the National Institute for Materials Science (NIMS) for the sample synthesis and x-ray diffraction measurements. We are grateful to Masamichi Nishino, Kazunari Yamaura, Alexei Belik, and Yoshihiro Tsujimoto at NIMS for fruitful discussions.

### APPENDIX: CALCULATION OF $I(\mathbf{Q})$

$I(\mathbf{Q})$  for the transition from the  $|\text{I}\rangle$  to the  $|\text{F}\rangle$  states is proportional to the following term:

$$\frac{k'}{k} \langle \text{I} | \hat{\mathbf{Q}}_{\perp}^+(\mathbf{Q}) | \text{F} \rangle \langle \text{F} | \hat{\mathbf{Q}}_{\perp}(\mathbf{Q}) | \text{I} \rangle \quad (\text{A1})$$

[23–26]. The parameters  $k$  and  $k'$  are the initial and final neutron wave numbers, respectively. The operator  $\hat{\mathbf{Q}}(\mathbf{Q})$  is expressed by the following equation:

$$\hat{\mathbf{Q}}(\mathbf{Q}) = f(\mathbf{Q}) \sum_{i=1}^8 \exp(i\mathbf{Q} \cdot \mathbf{R}_i) \mathbf{S}_i. \quad (\text{A2})$$

Here,  $f(\mathbf{Q})$  denotes the magnetic form factor of an isolated  $\text{Cu}^{2+}$  ion [27–29]. The position of the spin  $\mathbf{S}_i$  is indicated by  $\mathbf{R}_i$ . The center of two Cu4 sites connected by the  $J_4$

interaction, as shown in Fig. 1, is set as the origin of  $\mathbf{R}_i$ . The subscript  $\perp$  in Eq. (A1) indicates a projection onto a plane perpendicular to the scattering vector  $\mathbf{Q}$ . Since no magnetic order exists in  $\text{KCu}_4\text{P}_3\text{O}_{12}$ , we can consider that  $\hat{\mathbf{Q}}_{\perp}(\mathbf{Q}) = \hat{\mathbf{Q}}(\mathbf{Q})$ . Here, we express the matrix elements as follows:

$$\langle \text{F} | \hat{\mathbf{Q}}_{\perp}(\mathbf{Q}) | \text{I} \rangle_j = \sum_{i=1}^8 \exp(i\mathbf{Q} \cdot \mathbf{R}_i) a_{ji}, \quad j = x, y, z. \quad (\text{A3})$$

Note that the values of  $a_{ji}$  also depend on eigenstates ( $|\text{I}\rangle$  and  $|\text{F}\rangle$  states). We obtained that  $a_{ji} = a_{j(9-i)}$  ( $i = 1 \sim 4$ ) for the 0-1, 0-4, 1-3, and 1-4 excitations and that  $a_{ji} = -a_{j(9-i)}$  ( $i = 1 \sim 4$ ) for the 0-2 and 1-2 excitations. Therefore,

$$\begin{aligned} & \langle \text{I} | \hat{\mathbf{Q}}_{\perp}^+(\mathbf{Q}) | \text{F} \rangle \langle \text{F} | \hat{\mathbf{Q}}_{\perp}(\mathbf{Q}) | \text{I} \rangle \\ &= 4 \sum_{jii'} \cos(\mathbf{Q} \cdot \mathbf{R}_i) \cos(\mathbf{Q} \cdot \mathbf{R}_{i'}) a_{ji} a_{j'i'} \end{aligned} \quad (\text{A4})$$

for the 0-1, 0-4, 1-3, and 1-4 excitations and

$$\begin{aligned} & \langle \text{I} | \hat{\mathbf{Q}}_{\perp}^+(\mathbf{Q}) | \text{F} \rangle \langle \text{F} | \hat{\mathbf{Q}}_{\perp}(\mathbf{Q}) | \text{I} \rangle \\ &= 4 \sum_{jii'} \sin(\mathbf{Q} \cdot \mathbf{R}_i) \sin(\mathbf{Q} \cdot \mathbf{R}_{i'}) a_{ji} a_{j'i'} \end{aligned} \quad (\text{A5})$$

for the 0-2 and 1-2 excitations. After a spherical average,  $I(\mathbf{Q})$  is expressed as follows:

$$I(\mathbf{Q}) = f(\mathbf{Q})^2 \left[ \sum_{i \neq i'} A_{ii', \text{IF}} \left( \frac{\sin Q|\mathbf{R}_i - \mathbf{R}_{i'}|}{Q|\mathbf{R}_i - \mathbf{R}_{i'}|} + \frac{\sin Q|\mathbf{R}_i + \mathbf{R}_{i'}|}{Q|\mathbf{R}_i + \mathbf{R}_{i'}|} \right) + \sum_i A_{i, \text{IF}} \left( 1 + \frac{\sin 2Q|\mathbf{R}_i|}{2Q|\mathbf{R}_i|} \right) \right] \quad (\text{A6})$$

for the 0-1, 0-4, 1-3, and 1-4 excitations and

$$I(\mathbf{Q}) = f(\mathbf{Q})^2 \left[ \sum_{i \neq i'} A_{ii', \text{IF}} \left( \frac{\sin Q|\mathbf{R}_i - \mathbf{R}_{i'}|}{Q|\mathbf{R}_i - \mathbf{R}_{i'}|} - \frac{\sin Q|\mathbf{R}_i + \mathbf{R}_{i'}|}{Q|\mathbf{R}_i + \mathbf{R}_{i'}|} \right) + \sum_i A_{i, \text{IF}} \left( 1 - \frac{\sin 2Q|\mathbf{R}_i|}{2Q|\mathbf{R}_i|} \right) \right] \quad (\text{A7})$$

for the 0-2 and 1-2 excitations.  $A_{i, \text{IF}}$  is always positive because it consists of  $a_{ji}^2$ .  $A_{ii', \text{IF}}$  can be both positive and negative because it consists of  $a_{ji} a_{j'i'}$ . The dominant term in the 0-1

and 1-3 excitations is  $A_{3, \text{IF}} \left( 1 + \frac{\sin 2Q|\mathbf{R}_3|}{2Q|\mathbf{R}_3|} \right)$ . Therefore, the calculated  $I(\mathbf{Q})$  curves for the 0-1 and 1-3 excitations are similar to each other as shown in Fig. 8(a).

- [1] H. Kikuchi, Y. Fujii, M. Chiba, S. Mitsudo, T. Idehara, T. Tonegawa, K. Okamoto, T. Sakai, T. Kuwai, and H. Ohta, Experimental observation of the  $\frac{1}{3}$  magnetization plateau in the diamond-chain compound  $\text{Cu}_3(\text{CO}_3)_2(\text{OH})_2$ , *Phys. Rev. Lett.* **94**, 227201 (2005).
- [2] B. Gu and G. Su, Comment on ‘‘Experimental observation of the  $\frac{1}{3}$  magnetization plateau in the diamond-chain compound  $\text{Cu}_3(\text{CO}_3)_2(\text{OH})_2$ ’’, *Phys. Rev. Lett.* **97**, 089701 (2006).
- [3] H. Kikuchi, Y. Fujii, M. Chiba, S. Mitsudo, T. Idehara, T. Tonegawa, K. Okamoto, T. Sakai, T. Kuwai, and H. Ohta, Kikuchi *et al.* Reply, *Phys. Rev. Lett.* **97**, 089702 (2006).
- [4] B. Gu and G. Su, Magnetism and thermodynamics of spin-1/2 Heisenberg diamond chains in a magnetic field, *Phys. Rev. B* **75**, 174437 (2007).
- [5] K. C. Rule, A. U. B. Wolter, S. S ullow, D. A. Tennant, A. Br uhl, S. K ohler, B. Wolf, M. Lang, and J. Schreuer, Nature of the spin

- dynamics and  $\frac{1}{3}$  magnetization plateau in azurite, *Phys. Rev. Lett.* **100**, 117202 (2008).
- [6] J. Kang, C. Lee, R. K. Kremer, and M.-H. Whangbo, Consequences of the intrachain dimer-monomer spin frustration and the interchain dimer-monomer spin exchange in the diamond-chain compound azurite  $\text{Cu}_3(\text{CO}_3)_2(\text{OH})_2$ , *J. Phys.: Condens. Matter* **21**, 392201 (2009).
- [7] H. Jeschke, I. Opahle, H. Kandpal, R. Valent ı, H. Das, T. Saha-Dasgupta, O. Janson, H. Rosner, A. Br uhl, B. Wolf, M. Lang, J. Richter, S. Hu, X. Wang, R. Peters, T. Pruschke, and A. Honecker, Multistep approach to microscopic models for frustrated quantum magnets: The case of the natural mineral azurite, *Phys. Rev. Lett.* **106**, 217201 (2011).
- [8] K. C. Rule, M. Reehuis, M. C. R. Gibson, B. Ouladdiaf, M. J. Gutmann, J.-U. Hoffmann, S. Gerischer, D. A. Tennant, S. S ullow, and M. Lang, Magnetic and crystal structure of azurite

- $\text{Cu}_3(\text{CO}_3)_2(\text{OH})_2$  as determined by neutron diffraction, *Phys. Rev. B* **83**, 104401 (2011).
- [9] Y. C. Sun, Z. W. Ouyang, J. F. Wang, Z. X. Wang, Z. C. Xia, and G. H. Rao, Breaking of 1D magnetism in a spin-1 chain antiferromagnet  $\text{Ni}_2\text{V}_2\text{O}_7$ : ESR and first-principles studies, *Eur. Phys. J. Plus* **131**, 343 (2016).
- [10] Z. W. Ouyang, Y. C. Sun, J. F. Wang, X. Y. Yue, R. Chen, Z. X. Wang, Z. Z. He, Z. C. Xia, Y. Liu, and G. H. Rao, Novel half-magnetization plateau and nematiclike transition in the  $S = 1$  skew chain  $\text{Ni}_2\text{V}_2\text{O}_7$ , *Phys. Rev. B* **97**, 144406 (2018).
- [11] J. J. Cao, Z. W. Ouyang, X. C. Liu, T. T. Xiao, Y. R. Song, J. F. Wang, Y. Ishii, X. G. Zhou, and Y. H. Matsuda, Unusual dimerization and magnetization plateaus in  $S = 1$  skew chain  $\text{Ni}_2\text{V}_2\text{O}_7$  observed at 120 T, *Phys. Rev. B* **106**, 184409 (2022).
- [12] M. Hase, A. Dönni, N. Terada, V. Yu. Pomjakushin, J. R. Hester, K. C. Rule, and Y. Matsuo, Neutron diffraction studies under zero and finite magnetic fields of the  $\frac{1}{2}$  quantum magnetization plateau compound  $\text{Ni}_2\text{V}_2\text{O}_7$ , *Phys. Rev. B* **107**, 224415 (2023).
- [13] R. Tamura and K. Hukushima, Method for estimating spin-spin interactions from magnetization curves, *Phys. Rev. B* **95**, 064407 (2017).
- [14] R. Tamura and K. Hukushima, Bayesian optimization for computationally extensive probability distributions, *PLoS One* **13**, e0193785 (2018).
- [15] R. Tamura, K. Hukushima, A. Matsuo, K. Kindo, and M. Hase, Data-driven determination of the spin Hamiltonian parameters and their uncertainties: The case of the zigzag-chain compound  $\text{KCu}_4\text{P}_3\text{O}_{12}$ , *Phys. Rev. B* **101**, 224435 (2020).
- [16] H. Effenberger,  $\text{KCu}_4(\text{PO}_4)_3$ : A compound with two trigonal dipyramidal  $\text{Cu}(\text{II})\text{O}_5$  coordination polyhedra, *Z. Kristallogr.* **180**, 43 (1987).
- [17] K. Momma and F. Izumi, VESTA for three-dimensional visualization of crystal, volumetric and morphology data, *J. Appl. Crystallogr.* **44**, 1272 (2011).
- [18] J. Rodríguez-Carvajal, Recent advances in magnetic structure determination by neutron powder diffraction, *Phys. B: Condens. Matter* **192**, 55 (1993); <http://www.ill.eu/sites/fullprof/>.
- [19] S. Itoh, T. Yokoo, S. Satoh, S. Yano, D. Kawana, J. Suzuki, and T. J. Sato, High resolution chopper spectrometer (HRC) at J-PARC, *Nucl. Instrum. Methods Phys. Res., Sect. A* **631**, 90 (2011).
- [20] S. Yano, S. Itoh, T. Yokoo, S. Satoh, T. Yokoo, D. Kawana, and T. J. Sato, Data acquisition system for high resolution chopper spectrometer (HRC) at J-PARC, *Nucl. Instrum. Methods Phys. Res., Sect. A* **654**, 421 (2011).
- [21] S. Itoh, K. Ueno, and T. Yokoo, Fermi chopper developed at KEK, *Nucl. Instrum. Methods Phys. Res., Sect. A* **661**, 58 (2012).
- [22] R. E. Watson and A. J. Freeman, Hartree-Fock atomic scattering factors for the iron transition series, *Acta Crystallogr.* **14**, 27 (1961).
- [23] A. Furrer and H. U. Güdel, Interference effects in neutron scattering from magnetic clusters, *Phys. Rev. Lett.* **39**, 657 (1977).
- [24] S. W. Lovesey, *Theory of Neutron Scattering from Condensed Matter* (Clarendon, Oxford, 1984), Vol. 2.
- [25] A. Zheludev, G. Shirane, Y. Sasago, M. Hase, and K. Uchinokura, Dimerized ground state and magnetic excitations in  $\text{CaCuGe}_2\text{O}_6$ , *Phys. Rev. B* **53**, 11642 (1996).
- [26] M. Hase, K. M. S. Etheredge, S.-J. Hwu, K. Hirota, and G. Shirane, Spin-singlet ground state with energy gaps in  $\text{Cu}_2\text{PO}_4$ : Neutron-scattering, magnetic-susceptibility, and ESR measurements, *Phys. Rev. B* **56**, 3231 (1997).
- [27] J. Akimitsu and Y. Ito, Magnetic form factor of  $\text{Cu}^{2+}$  in  $\text{K}_2\text{CuF}_4$ , *J. Phys. Soc. Jpn.* **40**, 1621 (1976).
- [28] T. Freltoft, G. Shirane, S. Mitsuda, J. P. Remeika, and A. S. Cooper, Magnetic form factor of Cu in  $\text{La}_2\text{CuO}_4$ , *Phys. Rev. B* **37**, 137 (1988).
- [29] P. J. Brown, Magnetic form factors, in *International Tables for Crystallography*, Vol. C: Mathematical, physical and chemical tables, edited by E. Prince, Sec. 4.4.5 (Wiley and Hoboken, New Jersey, USA, 2006), pp. 454–461.